

SUPPORTING INFORMATION

Rational Design and Development of Lanthanide-doped NaYF₄@CdS-Au-RGO as Quaternary Plasmonic Photocatalysts for Harnessing Visible-NIR Broadband Spectrum

Ajay Kumar, Kumbam Lingeshwar Reddy, Suneel Kumar,

Ashish Kumar, Vipul Sharma and Venkata Krishnan*

School of Basic Sciences and Advanced Materials Research Center, Indian Institute of Technology Mandi, Kamand, Mandi 175005, Himachal Pradesh, India.

Email: vkn@iitmandi.ac.in

Sl. No.	Content	Page No.
1	TEM image and EDAX spectrum of Au NP (Figure S1)	S-4
2	XRD pattern of GO and RGO (Figure S2)	S-5
3	N ₂ adsorption-desorption isotherms, pore size distribution curves and BET surface area plots for UCNP, UC, UCA and UCAG4 nanocomposite (Figure S3)	S-6
4	Summary of specific surface area and pore volume distribution of UCNP, UC, UCA and UCAG4 nanocomposites (Table S1)	S-7
5	Elemental mapping and EDAX spectrum of UCAG4 (Figure S4)	S-8
6	XPS spectra of NaYF ₄ :Yb/Er@CdS-Au-RGO (a) survey spectrum (b) Position of the valance band edge (EVBM) and the intrinsic Fermi level (EF) of UCAG4 nanocomposite (Figure S5)	S-9
7	UV-vis spectra of (a) bare CdS, GO and Au NP, and (b) UCAG1, UCAG2, UCAG3, UCAG4 and UCAG5 nanocomposites (Figure S6)	S-10
8	PL spectra of CdS, UC, UCA, UCAG3 and UCAG4 (Figure S7)	S-11
9	DRS and plot of the transformed Kubelka–Munk function vs. the energy of light for CdS, UC, UCA, UCAG1, UCAG2, UCAG3, UCAG4 and UCAG5, respectively (Figure S8)	S-12
10	Structure of CFX molecule (Figure S9)	S-13
11	Photographs of pure CFX solution and UCAG4 in CFX solution (Figure S10)	S-14
12	Adsorption/degradation of CFX on UCAG4 nanocomposite under visible light irradiation (Figure S11)	S-15
13	Adsorption isotherm of CFX on UCAG4 nanocomposite (Figure S12)	S-16

14	Time dependent absorption spectra of CFX under visible irradiation (Figure S13)	S-17
15	Time dependent absorption spectra of CFX under NIR irradiation (Figure S14)	S-18
16	Summary of kinetic data of photocatalytic degradation of CFX under visible irradiation (Table S2)	S-19
17	Summary of kinetic data of photocatalytic degradation of CFX under NIR irradiation (Table S3)	S-20
18	Fitting of different models for kinetics of photocatalytic degradation of CFX using different catalysts under visible and NIR light irradiations (Figure S15)	S-21
19	Mass spectra of (a) CFX before degradation, and (b, c, d) degradation products of CFX after visible light irradiation for 180 min (Figure S16)	S-22
20	Summary of observed and calculated molecular ion masses of different fragments obtained by mass analysis and their proposed molecular structures (Table S4)	S-23

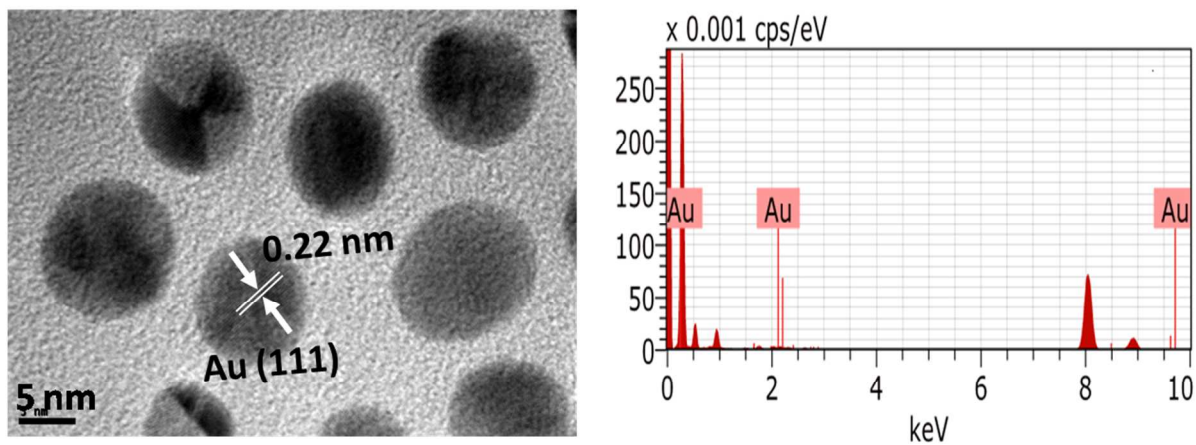


Figure S1. TEM image of Au NP (left). The interplanar distance of 0.22 nm can be indexed to the lattice spacing of the (111) plane of the face-centered cubic Au NP. EDAX spectrum of Au NP (right) is also given.

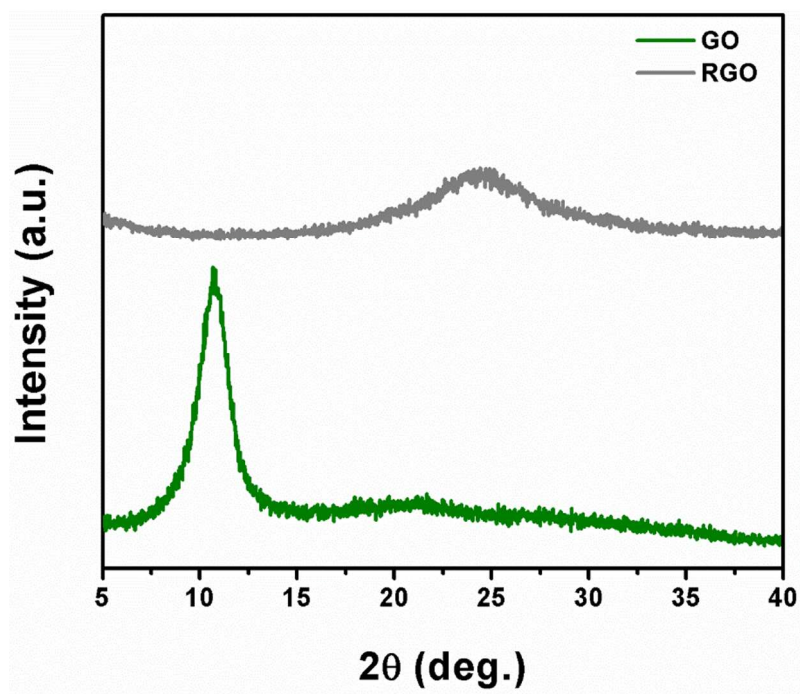


Figure S2. XRD pattern of GO and RGO.

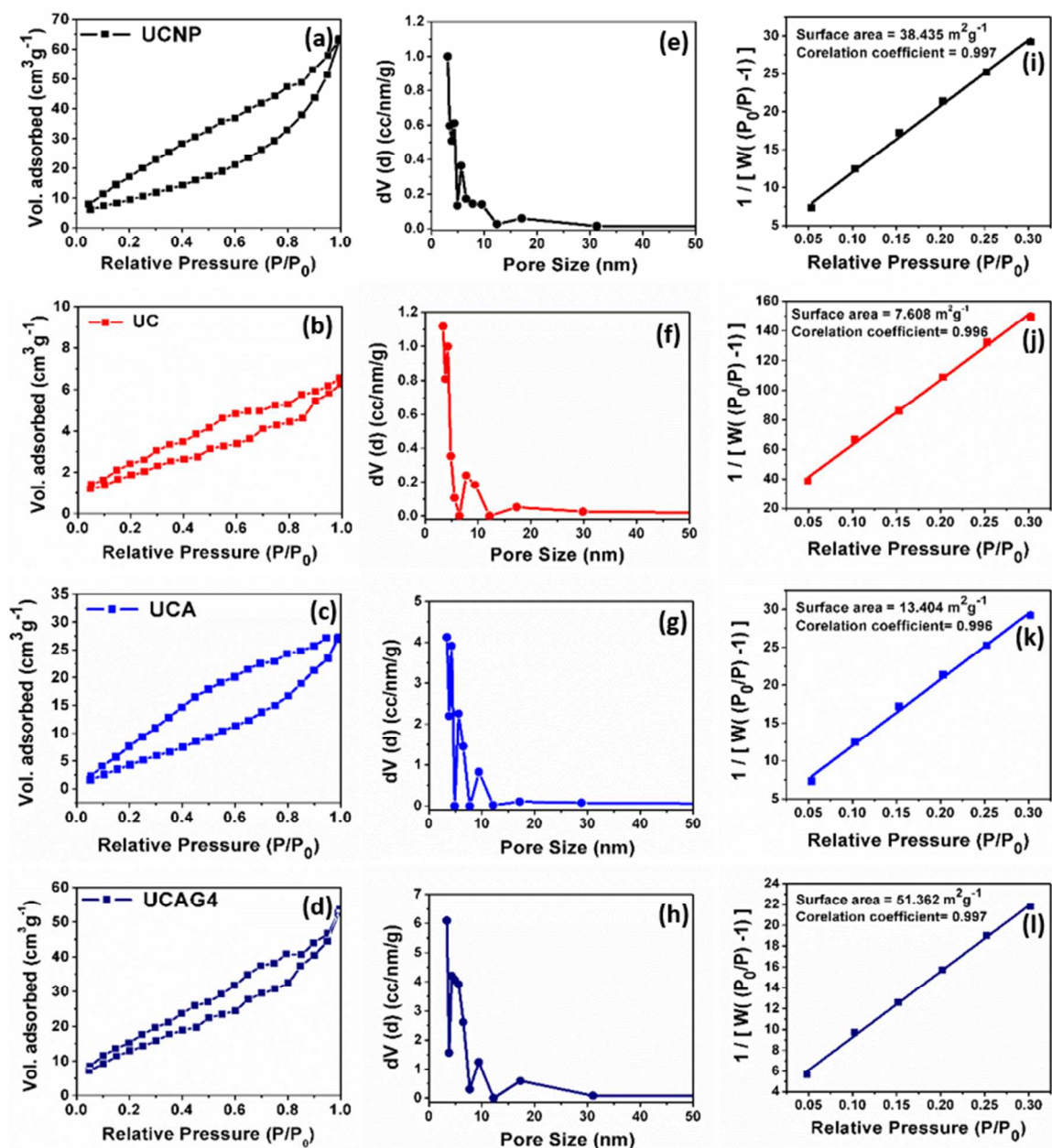


Figure S3. (a-d) N₂ adsorption-desorption isotherms, (e-h) pore size distribution curves and (i-l) BET surface area plots for UCNP, UC, UCA and UCAG4 nanocomposite, respectively.

Table S1. Summary of specific surface area and pore volume distribution of UCNP, UC, UCA and UCAG4 nanocomposites.

Sample	S_{BET} ($\text{m}^2 \text{g}^{-1}$)	Pore volume (cc g^{-1})
UCNP	38.435	0.083
UC	7.608	0.008
UCA	13.404	0.029
UCAG4	51.362	0.067

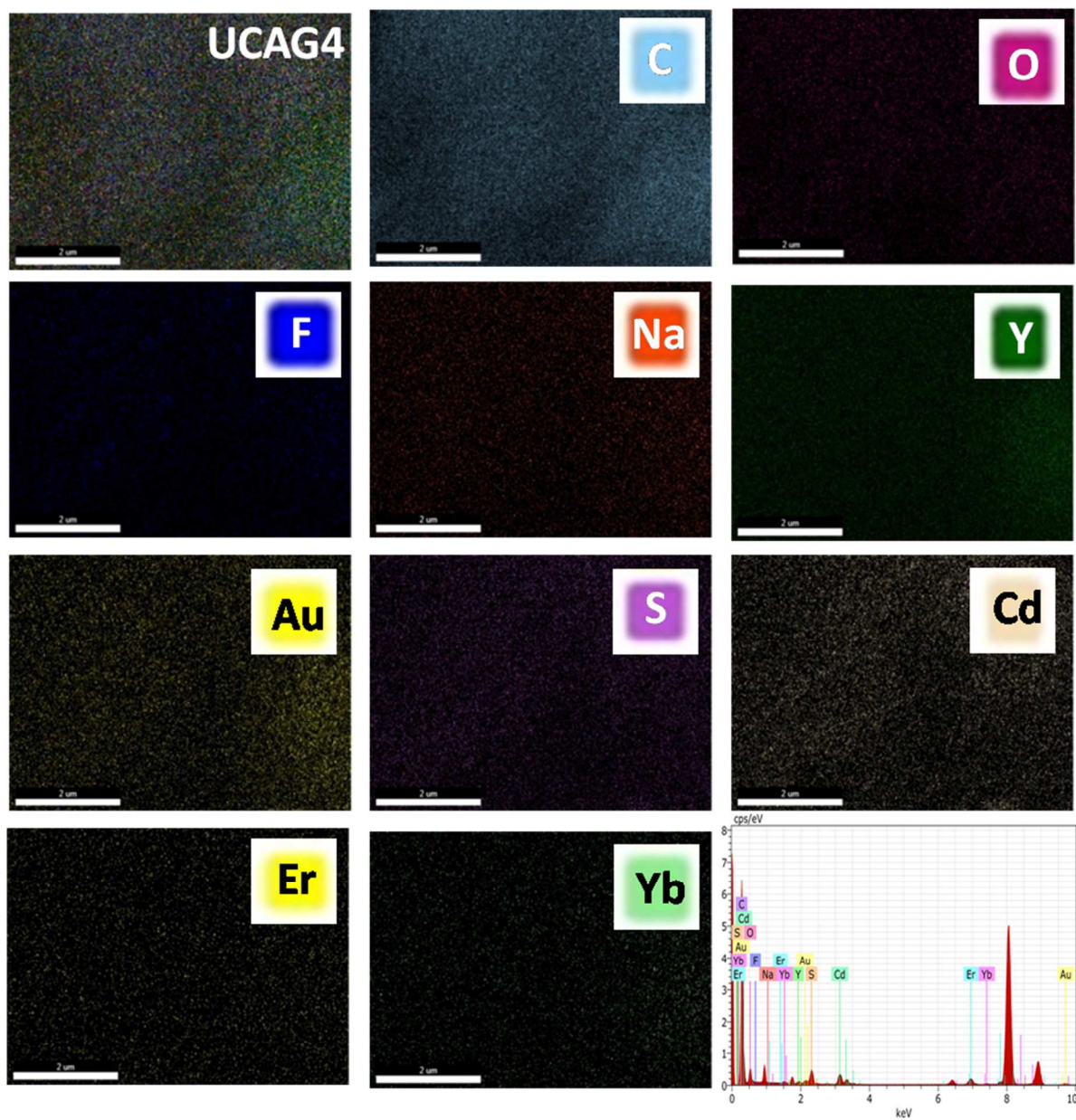


Figure S4. SEM elemental mapping and EDAX spectrum of UCAG4.

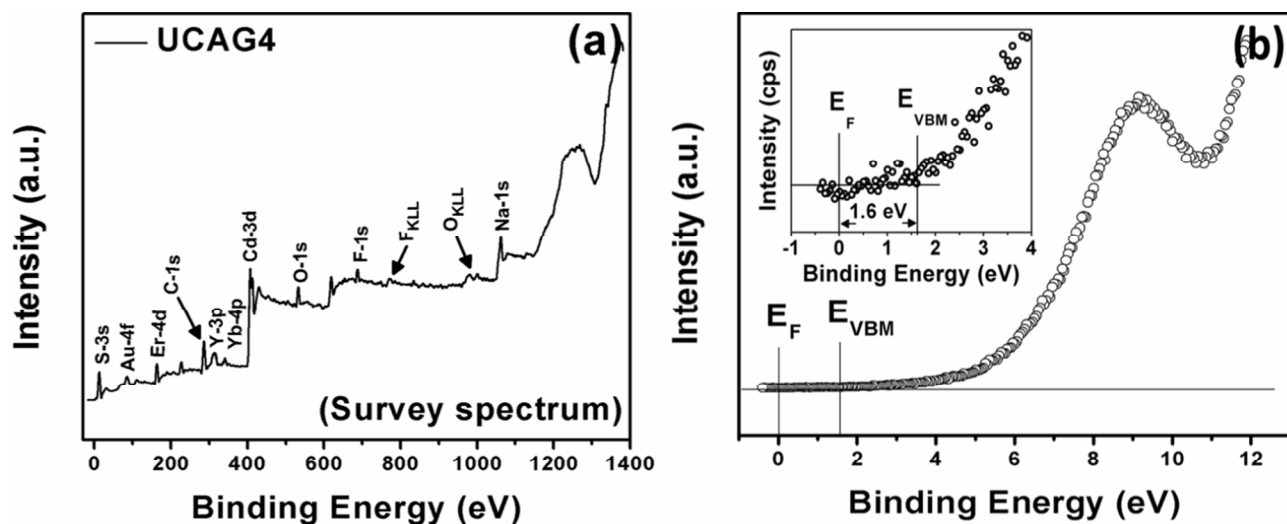


Figure S5. XPS for UCAG4 nanocomposite (a) survey spectrum, (b) position of the valance band edge (E_{VBM}) and the intrinsic Fermi level (E_F) of UCAG4 nanocomposite, wherein the magnified region of interest is shown in the inset.

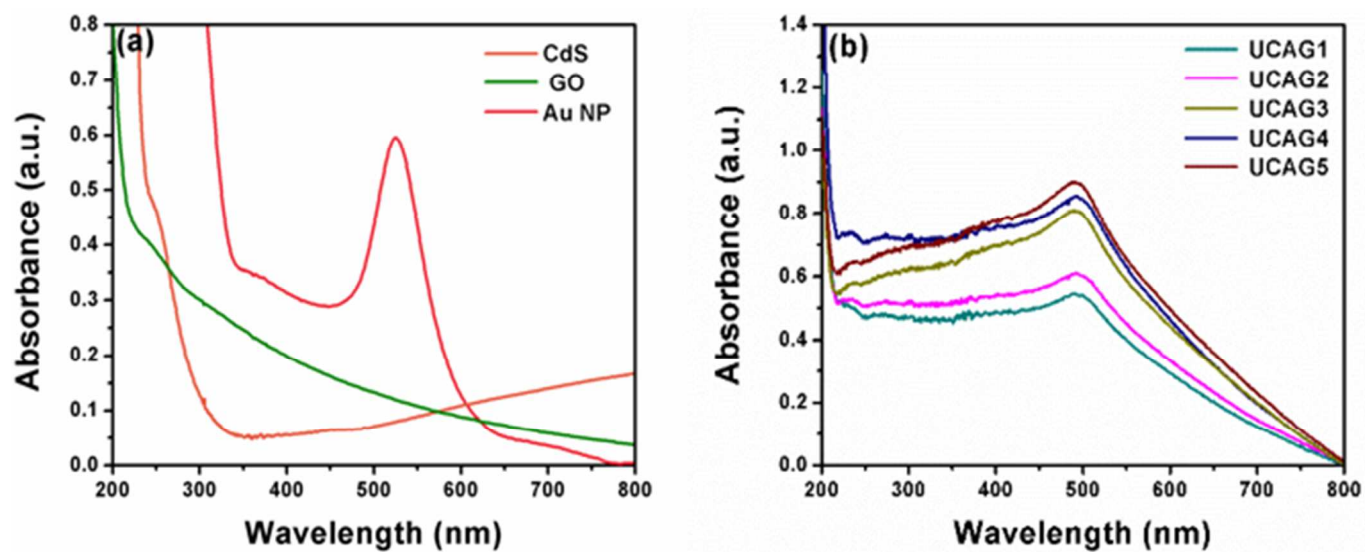


Figure S6. UV-vis spectra of (a) bare CdS, GO and Au NP, and (b) UCAG1, UCAG2, UCAG3, UCAG4 and UCAG5 nanocomposites.

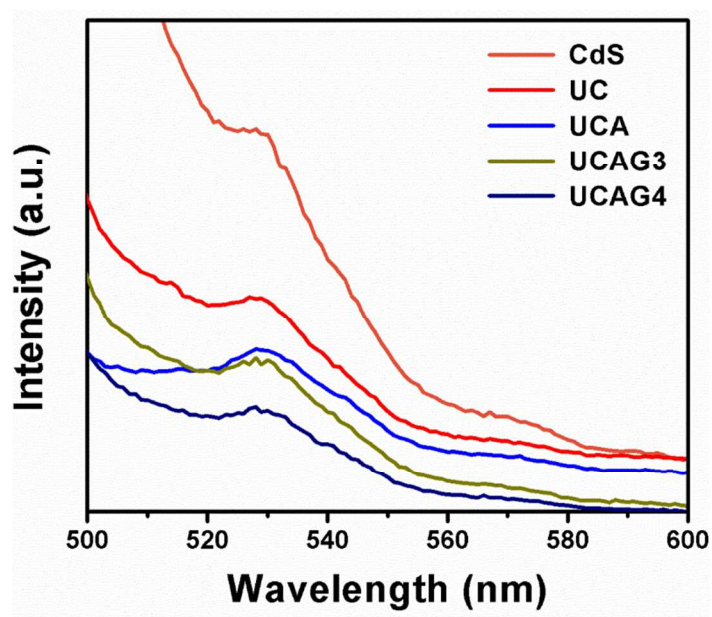


Figure S7. PL spectra of CdS, UC, UCA, UCAG3 and UCAG4.

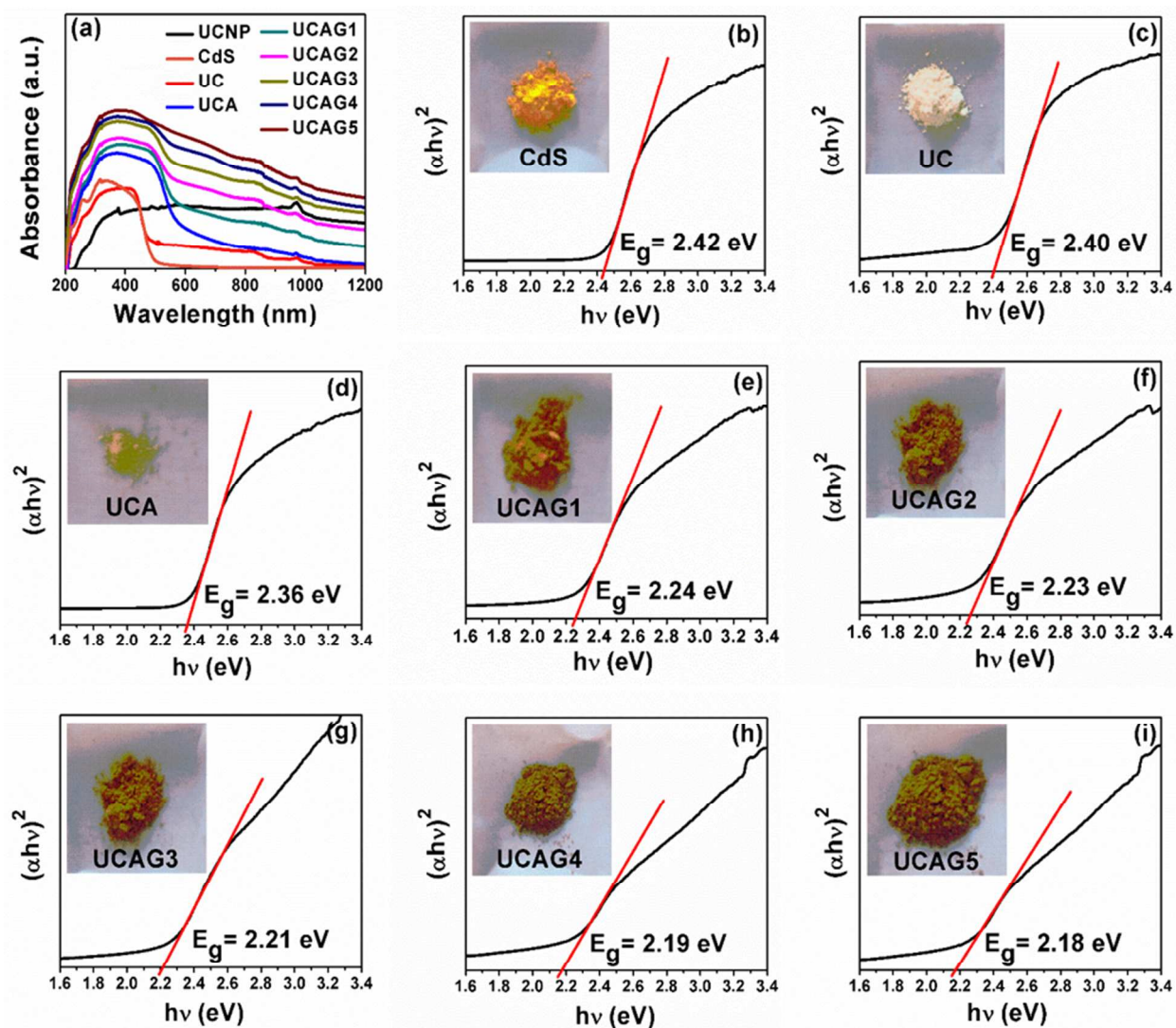


Figure S8. (a) DRS plot of CdS, UC, UCA, UCAG1, UCAG2, UCAG3, UCAG4 and UCAG5; (b-i) Plot of the transformed Kubelka–Munk function vs. the energy of light for CdS, UC, UCA, UCAG1, UCAG2, UCAG3, UCAG4 and UCAG5, respectively.

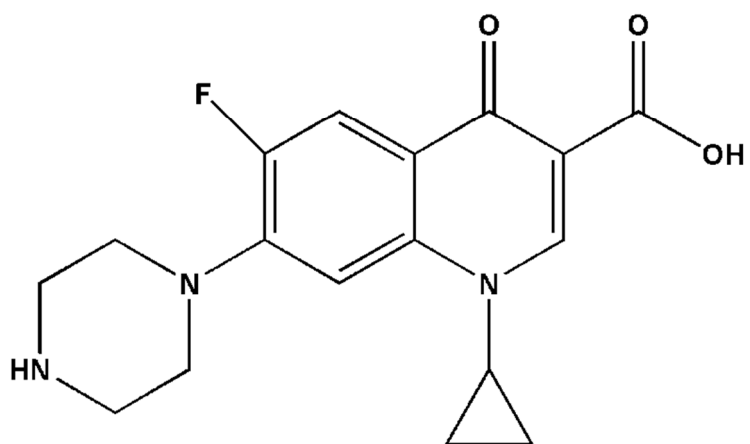


Figure S9. Structure of CFX molecule.

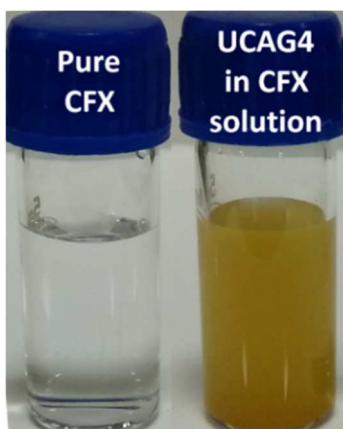


Figure S10. Photographs of pure CFX solution and UCAG4 in CFX solution clearly showing good dispersion of drug and UCAG4 nanocomposite.

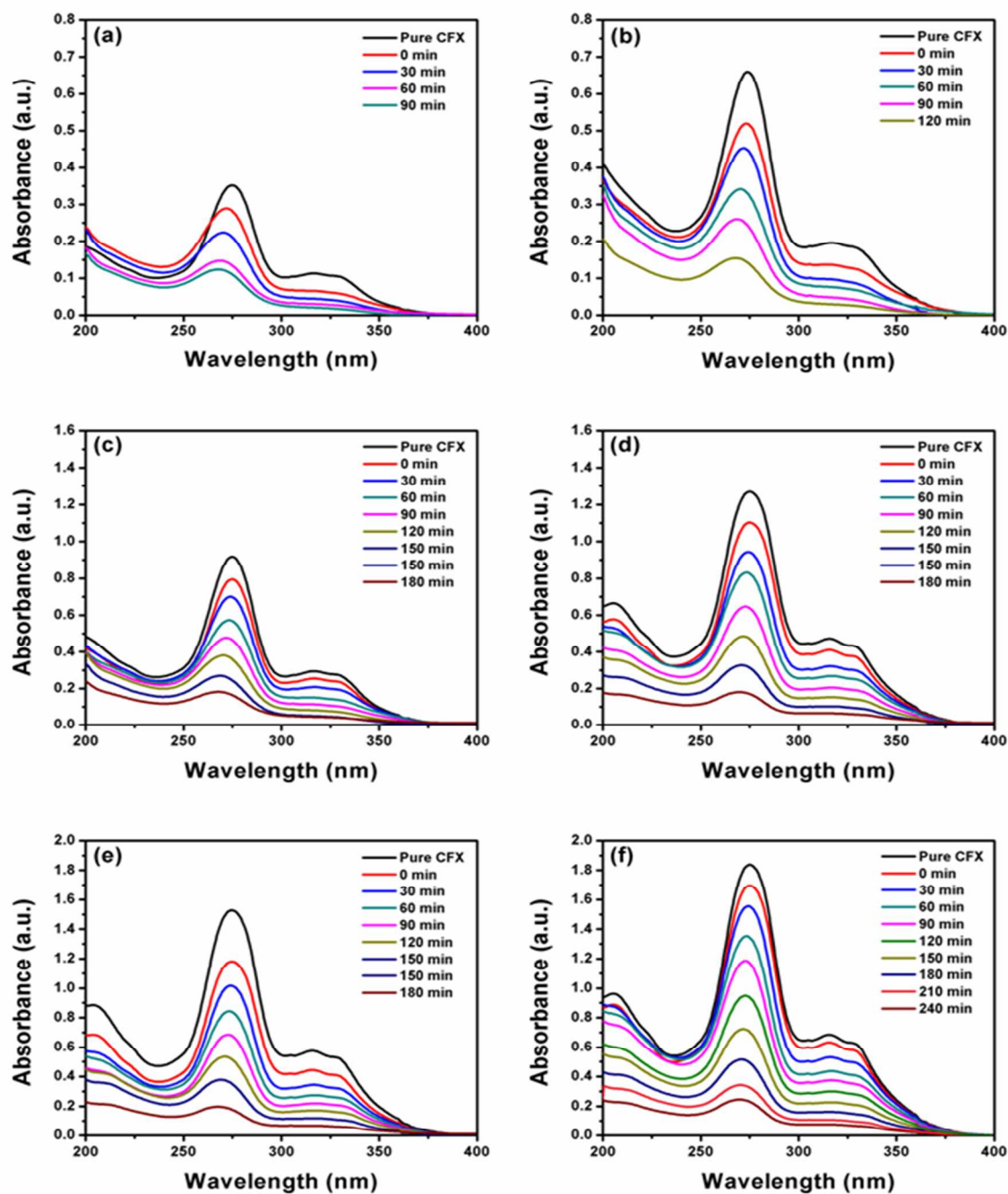


Figure S11. Adsorption/degradation of CFX on UCAG4 nanocomposite under visible light irradiation: (a) 10 μ M CFX (b) 20 μ M CFX (c) 30 μ M CFX (d) 40 μ M CFX (e) 50 μ M CFX and (f) 60 μ M CFX.

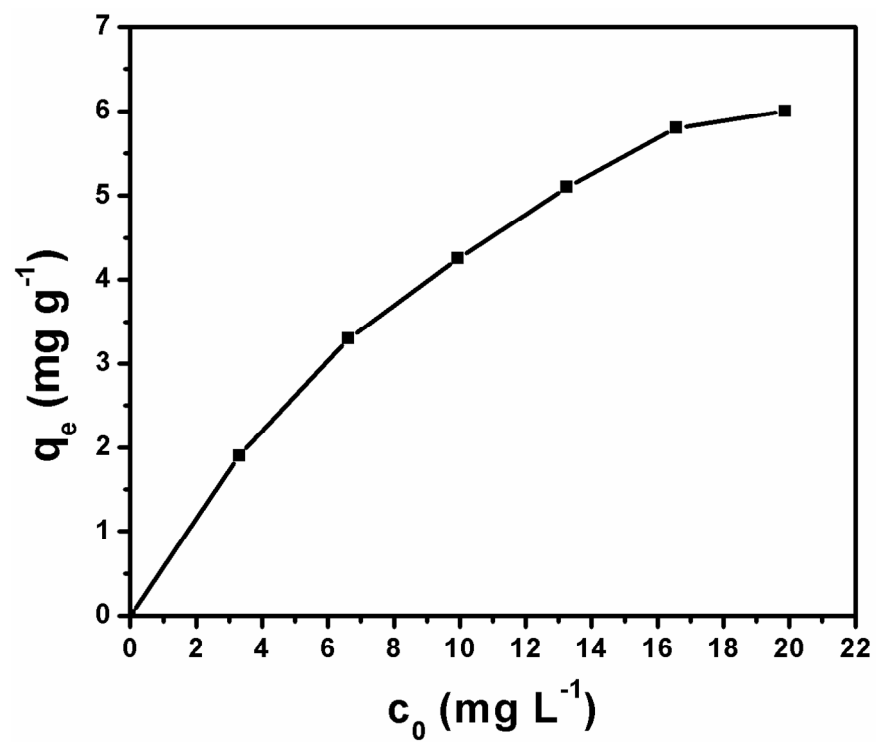


Figure S12. Adsorption isotherm of CFX on UCAG4 nanocomposite.

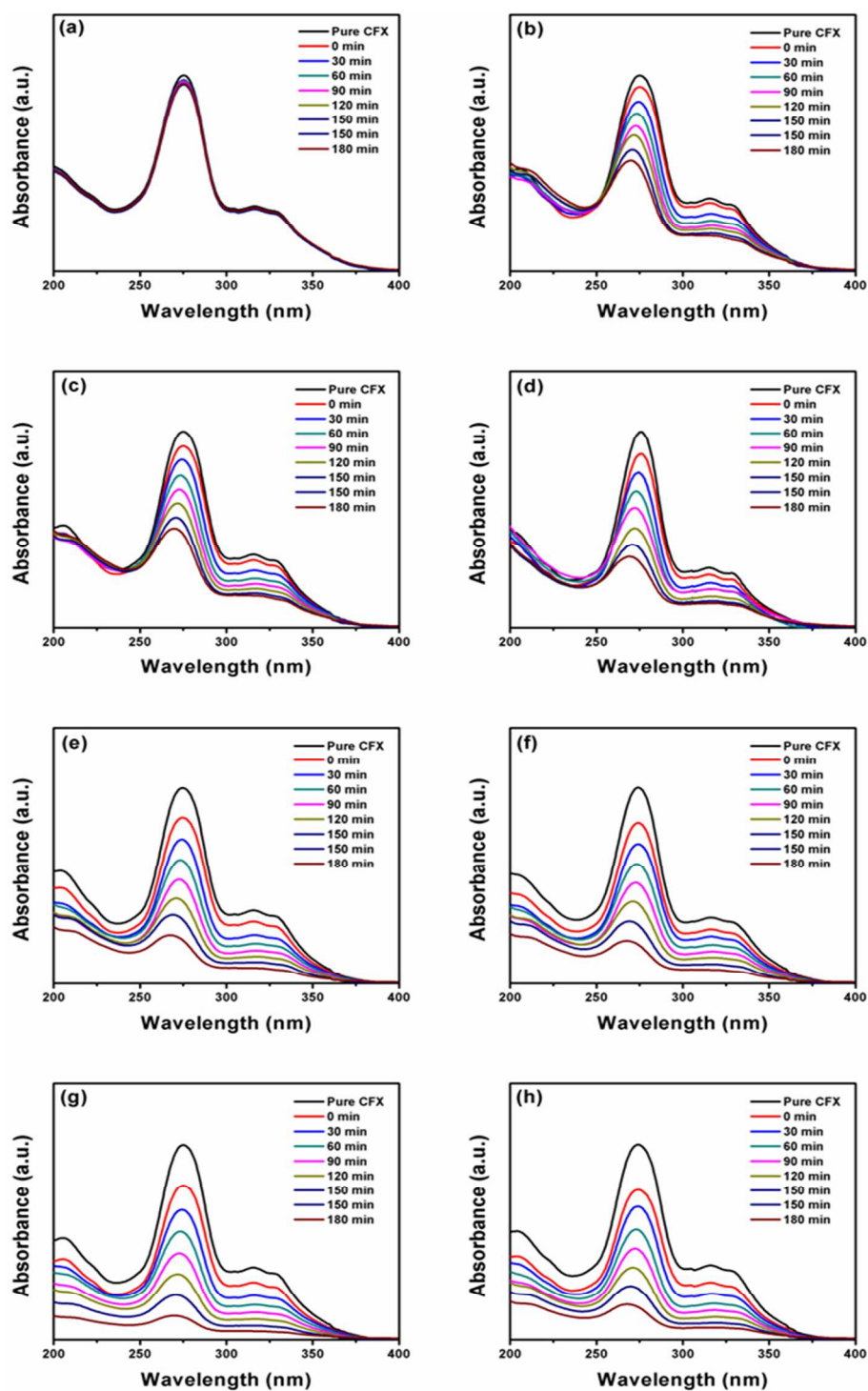


Figure S13. Time-dependent UV-vis spectra depicting the photocatalytic degradation of CFX under visible light irradiation: (a) UCNP, (b) UC, (c) UCA, (d) UCAG1, (e) UCAG2, (f) UCAG3, (g) UCAG4, and (h) UCAG5. Experimental conditions: CFX concentration 5×10^{-5} M, photocatalyst 6 mg per 15 mL and irradiation time 3 h.

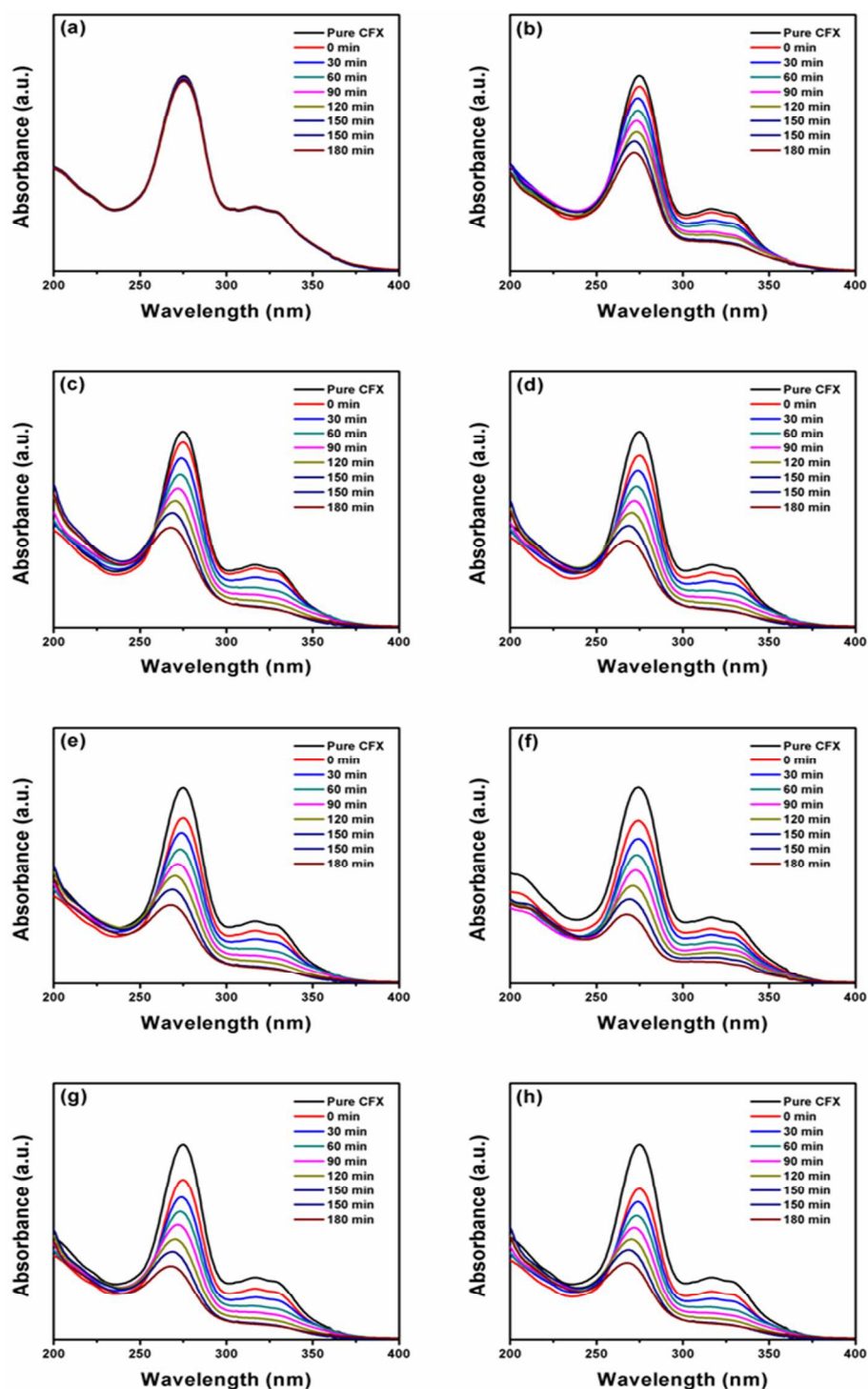


Figure S14. Time-dependent UV-vis spectra depicting the photocatalytic degradation of CFX under NIR light irradiation: (a) UCNP, (b) UC, (c) UCA, (d) UCAG1, (e) UCAG2, (f) UCAG3, (g) UCAG4, and (h) UCAG5. Experimental conditions: CFX concentration 5×10^{-5} M, photocatalyst 6 mg per 15 mL and irradiation time 3 h.

Table S2. Summary of kinetic data of photocatalytic degradation of CFX using all prepared photocatalysts under visible light irradiation

		UCNP	UC	UCA	UCAG1	UCAG2	UCAG3	UCAG4	UCAG5
Zero Order	R^2	0.880	0.998	0.999	0.998	0.996	0.993	0.988	0.981
	$k \times 10^{-3} \text{ (min}^{-1}\text{)}$	0.3	3.5	3.9	4.9	5.6	5.7	6.2	5.8
Pseudo First Order	R^2	0.880	0.998	0.999	0.982	0.966	0.952	0.926	0.954
	$k \times 10^{-3} \text{ (min}^{-1}\text{)}$	2.0	3.0	3.6	5.3	6.9	7.4	9.6	8.2
Parabolic diffusion model	R^2	0.941	0.967	0.995	0.992	0.987	0.980	0.985	0.993
	$k \times 10^{-3} \text{ (min}^{-1}\text{)}$	4.7	17.6	22.3	29.8	40.8	46.8	57.0	54.8
Modified Freundlich model	R^2	0.976	0.987	0.997	0.995	0.989	0.983	0.986	0.992
	$k \times 10^{-3} \text{ (min}^{-1}\text{)}$	3.0	11.9	15.9	21.7	31.5	37.6	49.0	43.4

Table S3. Summary of kinetic data of photocatalytic degradation of CFX using all prepared photocatalysts under NIR light irradiation

		UCNP	UC	UCA	UCAG1	UCAG2	UCAG3	UCAG4	UCAG5
Zero	R^2	0.785	0.978	0.974	0.977	0.973	0.971	0.964	0.938
Order	$k \times 10^{-3} \text{ (min}^{-1}\text{)}$	0.1	3.0	4.0	4.2	4.4	4.7	4.5	4.3
Pseudo	R^2	0.787	0.993	0.981	0.987	0.986	0.982	0.988	0.985
First Order	$k \times 10^{-3} \text{ (min}^{-1}\text{)}$	0.1	2.6	3.8	4.3	4.7	5.3	5.0	4.7
Parabolic	R^2	0.939	0.989	0.993	0.985	0.986	0.980	0.979	0.984
diffusion model	$k \times 10^{-3} \text{ (min}^{-1}\text{)}$	2.7	15.2	23.0	31.4	37.9	44.9	42.3	38.8
Modified	R^2	0.979	0.995	0.997	0.989	0.988	0.981	0.976	0.978
Freundlich model	$k \times 10^{-3} \text{ (min}^{-1}\text{)}$	2.8	9.5	12.8	24.1	31.1	38.5	35.9	32.8

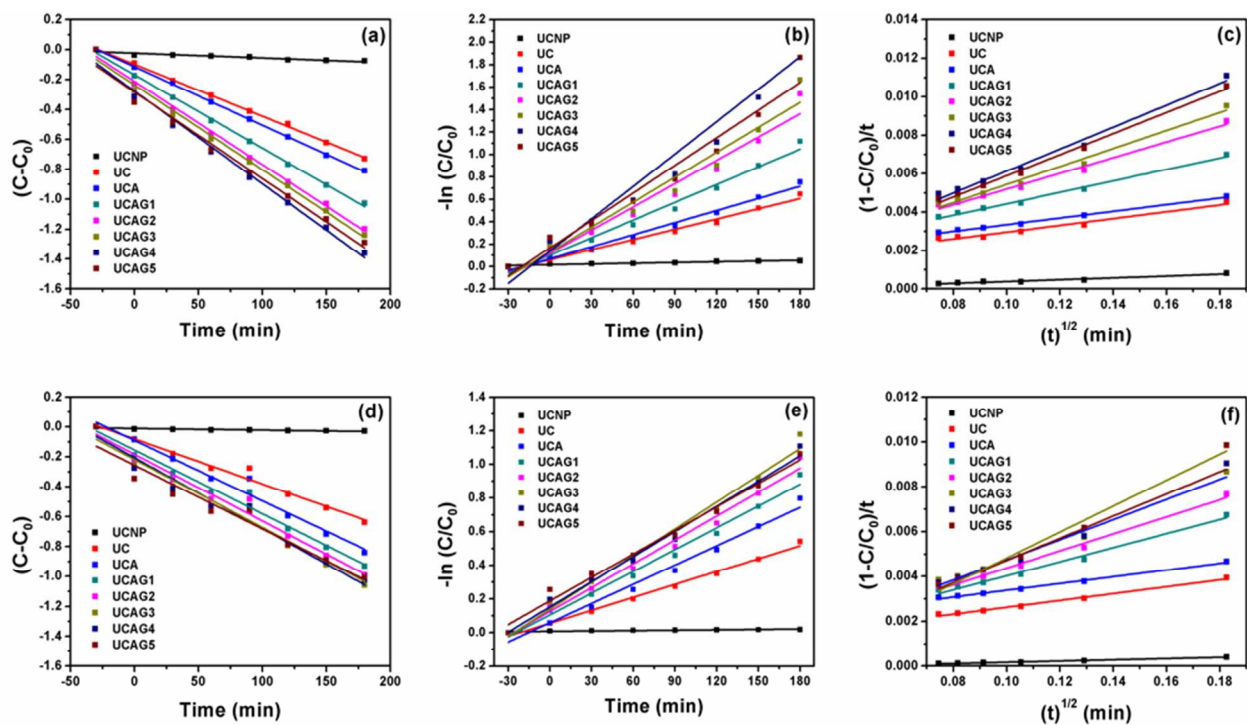


Figure S15. Fitting of different models for photocatalytic degradation kinetics under visible light (a) zero-order, (b) first-order, (c) parabolic diffusion model and under NIR light (d) Zero-order, (e) first-order, (f) parabolic diffusion model.

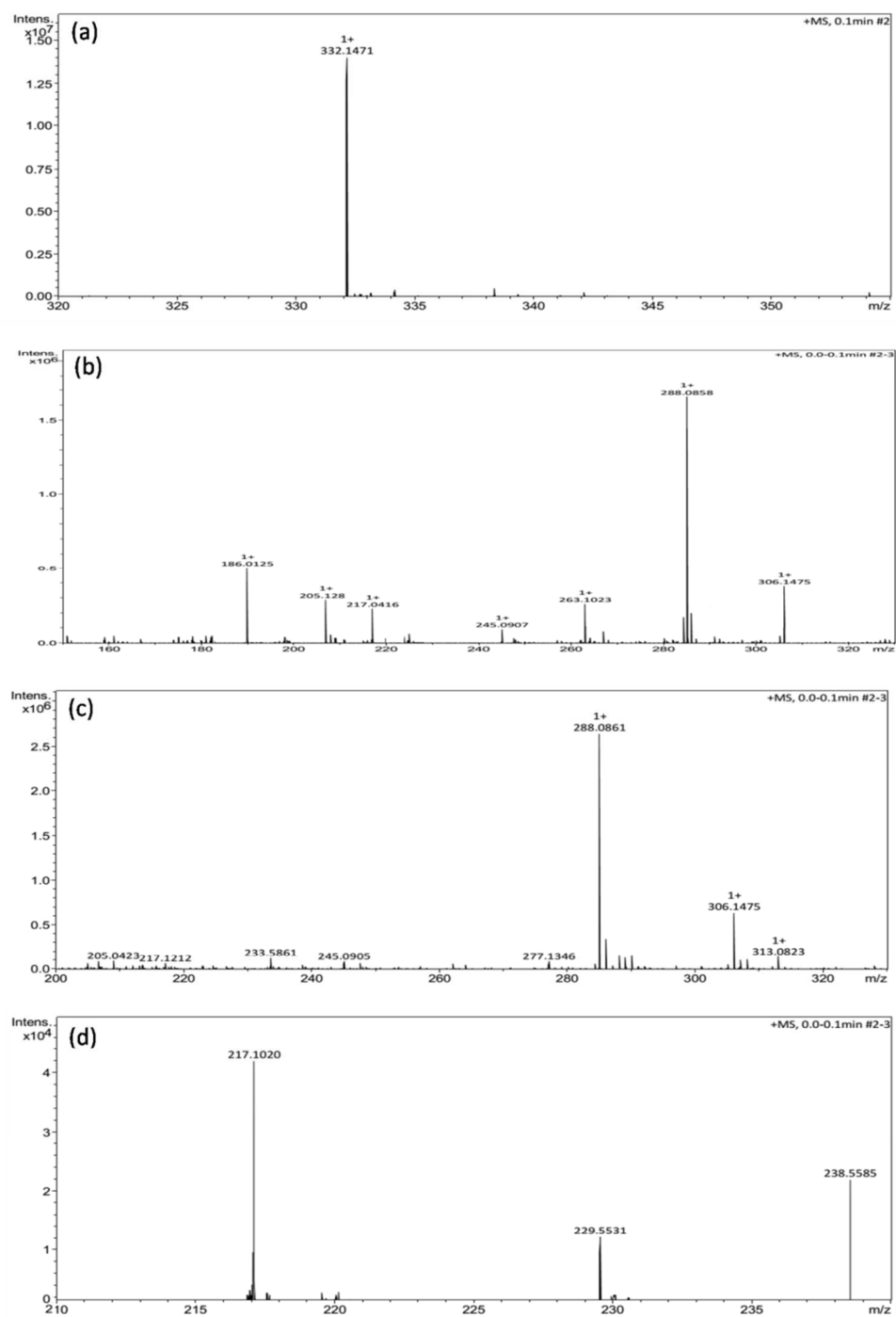
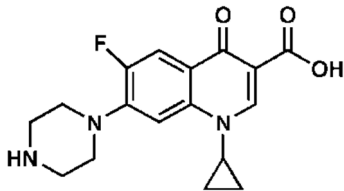
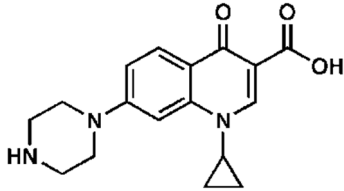
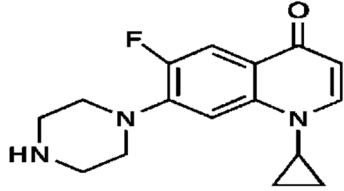
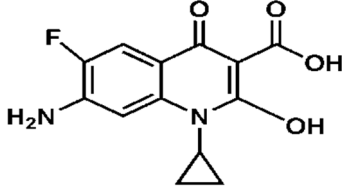
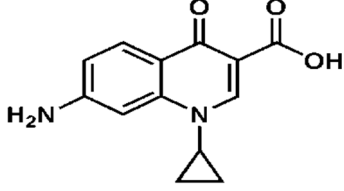
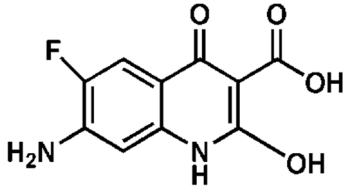
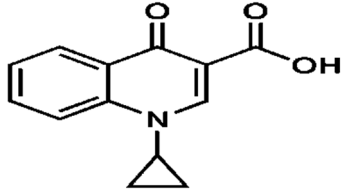
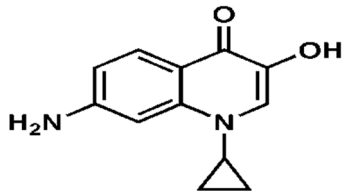
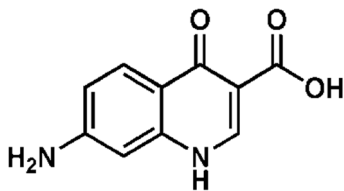


Figure S16. Mass spectra of (a) CFX before degradation, and (b, c, d) degradation products of CFX after visible light irradiation for 180 min.

Table S4. Summary of observed and calculated molecular ion masses of different fragments obtained by mass analysis and their proposed molecular structures.

ID of intermediate	Molecular formula	m/z (observed)	m/z (calculated)	Molecular structure
CFX	$C_{17}H_{18}FN_3O_3$	332.14	331.27	
P1	$C_{17}H_{19}N_3O_3$	313.08	313.14	
P2	$C_{16}H_{18}FN_3O$	288.08	287.33	
P3	$C_{13}H_{11}FN_2O_4$	277.13	278.07	
P4	$C_{13}H_{12}N_2O_3$	245.09	244.23	

P5	$C_{10}H_7FN_2O_4$	238.56	238.04	
P6	$C_{13}H_{11}NO_3$	229.55	229.07	
P7	$C_{12}H_{12}FN_2O_2$	217.10	216.29	
P8	$C_{10}H_8N_2O_3$	205.13	204.25	
P9	$C_{12}H_{11}NO$	186.01	185.22	